Inorg. Chem. **2007**, *46*, 4138–4144

$M_2Ba_2Sn_6$ (M = Yb, Ca): Metallic Zintl Phases with a Novel Tin Chain Substructure

Ming-Hui Ge and John D. Corbett*

Ames Laboratory, DOE and Department of Chemistry, Iowa State University, Ames, Iowa 50010

Received January 10, 2007

The compounds $M_2Ba_2Sn_6$ (M = Yb, Ca) have been synthesized by solid-state reactions in welded Ta tubes at high temperature. Their structures were determined by single-crystal X-ray diffraction studies to be orthorhombic; space group *Cmca* (No. 64); Z = 8; a = 15.871(3), 15.912 (3) Å; b = 9.387(2), 9.497(2) Å; c = 17.212(3), 17.184(3) Å; and V = 2564.3(9), 2597.0(9) Å^3, respectively. These contain infinite tin chains along $\vec{a}$ constructed from butterflylike 3-bonded Sn tetramers interconnected by pairs of 2-bonded Sn. The chains are further interconnected into corrugated layers by somewhat longer Sn–Sn bonds along $\vec{c}$. The compounds with the chains alone would be Zintl phases, but the interchain bonding makes them formally one-electron rich per formula unit. The electronic structures calculated by extended Hückel and TB-LMTO-ASA methods indicate that these compounds are metallic but with a deep pseudogap at the Fermi level. States that bind the extra electrons lie just below E_F and involve important Yb(Ca)–Sn contributions. The origin of metallic Zintl phases is briefly discussed.

Introduction

Solid-state chemistry has been intensively studied for a long time. Tin, on the boundary between metals and nonmetals, yields diverse types of compounds when combined with either more electropositive or more electronegative elements. The stannides that form on combination with the active metals are interesting because of their diverse structures, novel bonding, and interesting properties, especially those phases that qualify as Zintl phases.[1,2] Ideally, Zintl phases are valence compounds with well-defined relationships between the proportions of the active metal and the p element and their consequent bonding and electronic structures, namely, the octet rule is obeyed for all atoms in the anions. Accordingly, such Zintl phases are ideally diamagnetic semiconductors when complete valence electron transfer from the cations is assumed (Zintl−Klemm concept). Of course, these circumstances regard only the optimal relationships, and other factors may enter into the compositions, stabilities, and properties.

Tin is very diverse in the formation of nominal Zintl phases in either homoatomic or heteroatomic polyanions in binary or higher-order systems.[3,4] Many compounds are obtained in alkali metal−tin systems.[5] Perhaps the most famous examples are the tetrahedral anions, $[Sn_4]^{4-}$, which occur in ASn (A = Na, K, Rb, Cs)[6] and, in part, in $A_{52}Sn_{82}$ (A = K, Cs)[7] and $A_{12}Sn_{17}$ (A = K, Rb, Cs).[8] Zintl phases in these systems also include the condensed pentagonal dodecahedra of tin in K_8Sn_{25},[9] the defect clathrate structures in

* To whom correspondence should be addressed. E-mail: jcorbett@iastate.edu.

(1) (a) Eisenmann, B.; Cordier, G. In *Chemistry, Structure and Bonding of Zintl Phases and Ions*; Kauzlarich, S. M., Ed.; VCH Publishers: New York, 1996; p 61. (b) Corbett, J. D. In *Chemistry, Structure and Bonding of Zintl Phases and Ions*; Kauzlarich, S. M., Ed.; VCH Publishers: New York, 1996; p 139.
(2) Corbett, J. D. *Angew. Chem., Int. Ed.* **2000**, *39*, 670.
(3) Ganguli, A. K.; Corbett, J. D.; Köckerling, M. *J. Am. Chem. Soc.***1998**, *120*, 1223.
(4) Sun, Z.-M.; Xia, S.-Q.; Huang, Y.-Z.; Wu, L.-M.; Mao, J.-G. *Inorg. Chem.* **2005**, *44*, 9242.
(5) (a) Bobev, S.; Sevov, S. C. *Inorg. Chem.* **2000**, *39*, 5930. (b) Bobev, S.; Sevov, S. C. *Angew. Chem., Int. Ed.* **2000**, *39*, 4108. (c) Bobev, S.; Sevov, S. C. *Inorg. Chem.* **2001**, *40*, 5361. (d) Bobev, S.; Sevov, S. C. *J. Alloy Compd.* **2002**, *338*, 87. (e) Bobev, S.; Sevov, S. C. *J. Am. Chem. Soc.* **2002**, *124*, 3359.
(6) (a) Müller, W.; Volk, K. *Z. Naturforsch.* **1977**, *32b*, 709. (b) Hewaidy, I. F.; Busmann, E.; Klemm, W. *Z. Anorg. Allg. Chem.* **1964**, *328*, 283. (c) Baitinger, M.; Grin, Yu. N.; von Schnering, H. G.; Kniep, R.; Hrin, Yu. N. *Z. Kristallogr.−New Cryst. Struct.* **1999**, *214*, 457. (d) Baitinger, M.; Grin, Yu. N.; von Schnering, H. G.; Kniep, R.; Hrin, Yu. N. *Z. Kristallogr.−New Cryst. Struct.* **1999**, *214*, 457.
(7) Hoch, C.; Wendorff, M.; Röhr, C. *Z. Anorg. Allg. Chem.* **2003**, *629*, 2391.
(8) Hoch, C.; Wendorff, M.; Röhr, C. *J. Alloys Compd.* **2003**, *361*, 206.
(9) (a) Zhao, J.-T.; Corbett, J. D. *Inorg. Chem.* **1994**, *33*, 5721. (b) Dronskowski, R. Ph.D. Dissertation, University of Stuttgart, Stuttgart, Germany, 1990. (c) von Schnering, H.-G.; Kröner, R.; Baittinger, M.; Peters, K.; Nesper, R.; Grin, Y. *Z. Kristallogr.−New Cryst. Struct.* **2000**, *215*, 205. (d) Dubois, F.; Fässler, T. F. *J. Am. Chem. Soc.* **2005**, *127*, 3264.

10.1021/ic070042p CCC: $37.00
Published on Web 04/19/2007

A_8Sn_{44} (A = Rb, K, Cs),[9] and the complex 2D polyanions of realgar-type units $[Sn_8]^{4-}$ in $NaSn_2$,[10] etc. Diversity becomes even greater when mixed alkali metals or alkaline-earth metals are introduced into alkali metal−tin systems, essentially because of the increased opportunities to achieve well-packed lattices. For example, Zintl compounds $MNa_{10}Sn_{12}$ (M = Ca, Sr)[11a] contain isolated clusters of Sn_{12}^{12-} in the shape of giant truncated tetrahedra. Another Zintl phase example Na_8MSn_6 (M = Ba, Eu), even contains cyclopentadienyl-like anions Sn_5^{6-}.[11b] So far, tin substructures occur mainly as clusters or networks. Of course, these simple Zintl assignments do not ensure that the phases are actually closed shell and semiconducting in the dense solid state. Their properties have not been measured in many cases.

On the other hand, new phases and structures in the alkaline-earth metal (Ae)−tin systems, Zintl or not, do not appear to be plentiful, especially when the developments in recent years are considered. A limited number of compounds in these binary systems have been reported, mostly before 1980.[12] Only a few binary compounds have been reported since: Ae_3Sn_5 (Ae = Sr, Ba, Yb)[13] (electron rich, metallic Zintl phases), $Yb_{36}Sn_{23}$[14] (poor metal), $SrSn_3$[15] (metallic), and $SrSn_4$ (metallic, superconductor at 4.8 K, 10G).[16] Only one old example of a ternary phases is known in the Ca−Ba−Sn system, CaBaSn[17] with isolated tin atoms in an anti-$PbCl_2$-type structure, a closely related analogue of Ca_2Sn (Co_2Si-type),[18] both with a presumed oxidation state of −4 for the isolated tin atoms. Several binary phases that have been assigned as Zintl phases are known between tin and alkaline-earth or rare-earth (R) metals. The earliest reported AeSn (Ae = Ca or Ba) crystallizes as a CrB-type, the structure of which contains planar zigzag chains $_\infty^1[Sn^{2-}]$.[19] Such two-bonded Sn^{2-} atoms might be expected to fulfill the $8 - N$ rule, although theoretically such a simple condition does not seem likely.[20] The novel $Ca_{31}Sn_{20}$ is a rather complex Zintl phase with tin dimers, linear pentamers, and isolated tin in the structure. The assignment of classical two-center−two-electron bonds to the Sn−Sn interactions indicates that this compound is an electron-precise Zintl phase, in accordance with its diamagnetic susceptibility and semiconductive properties.[21] On the other hand, $Yb_{36}Sn_{23}$, containing a linear tin hexamer, as well as dimers and isolated tin atoms, also has a closed-shell oxidation state count and a Zintl phase classification, but electrical conductivity measurements show that it is a poor metal,[14] perhaps because of more dominant d-orbital bonding with that cation.

We report here the results of synthetic explorations of some Ae−R−Tt (R = Eu, Yb; Tt = Sn, Pb) systems, and the crystal structures and bonding analyses of $M_2Ba_2Sn_6$ (M = Yb, Ca). These turn out to be metallic (electron-rich) Zintl phases, but bonding analyses reveal these two compounds are well-bonded and exhibit pseudogaps at their Fermi levels.

Experimental Section

Syntheses. The starting materials for the preparation of $Yb_2Ba_2Sn_6$ and $Ca_2Ba_2Sn_6$ were the pure metals barium, strontium, tin (Alfa Aesar, purity ≥99.9%), and ytterbium (Ames Laboratory, purity ≥99.9% total). All manipulations were performed in a nitrogen-filled glovebox with a moisture level below 0.1 ppm. $Yb_2Ba_2Sn_6$ was initially obtained from a $YbBa_2Sn_5$ composition that was loaded into a tantalum tube already sealed at one end, subsequently arc-welded under an argon atmosphere, and finally sealed in an evacuated silica tube. This sample was first heated to 940 °C and held for 12h. The temperature was decreased to 700 °C at a rate of 2 °C/h and held there for 148 h. About 75% $Yb_2Ba_2Sn_6$ was present in the products. Powder XRD and single-crystal X-ray analyses of the other phases revealed that they were Sn and $Ba_xYb_{3-x}Sn_5$ (Pu_3Pd_5-type, *Cmcm*). The latter phases contain two extra electrons beyond Zintl assignments and are metallic.[13]

After the structure analysis, $Yb_2Ba_2Sn_6$ was prepared by reaction of a stoichiometric mixture of the metals at 940 °C for 12 h, followed by cooling to 650 °C at the rate of 5 °C/h. The sample was held at this temperature for 148 h and finally slowly cooled to room temperature at the rate of 5 °C/h. Several reactions were tried under different conditions, but all of them contain $Ba_xYb_{3-x}Sn_5$ and tin as secondary phases. The highest yield of $Yb_2Ba_2Sn_6$ was 80%. Similarly, $Ca_2Ba_2Sn_6$ was obtained from a stoichiometric reaction of the metals at 900 °C for 12 h, followed by cooling to 600 °C at 5 °C/h. The sample was held at this temperature for 148 h and finally slowly cooled to room temperature at 5 °C/h. Several reactions were run, but $Ba_xCa_{3-x}Sn_5$ was found as the secondary phase in the products; the highest yield of $Ca_2Ba_2Sn_6$ was ∼70%. The close proportions in A_3Sn_5 (Sn/A = 1.67) and $Ba_2M_2Sn_6$ (Sn/A = 1.50) and their unknown melting characteristics made it difficult to synthesize pure phases. The structural solutions are unambiguous as to the correct compositions, however.

Preliminary synthetic trials in the systems Ba−Eu−Sn, Sr−Yb−Sn, Mg−Ca−Sn, Sr−Ca−Sn, Ba−Yb−Pb, Sr−Ba−Pb, Ba−Ca−Pb, Sr−Ca−Pb, and Sr−Yb−Pb failed to gain any orthorhombic $A_2A'_2Sn_6$ phase, rather *Cmcm* $A_xA'_{3-x}Sn_5$ phases were found to be the main products. These suggest that the packing of ytterbium or calcium with barium and the Sn array is optimal and essential to the stability of the title phases.

Powder X-ray Diffraction. X-ray powder diffraction patterns were obtained from samples mounted between pieces of Mylar in the glovebox to protect them from the atmosphere. A Huber 670 Guinier Powder camera equipped with an area detector and Cu Kα radiation (λ = 1.540 598 Å) was employed to obtain useful data. The best experimental powder patterns showed 70−80% $M_2Ba_2Sn_6$ for both with narrow peaks and no deviations from the calculated powder patterns. Only one major secondary peak at about 32° was found in the best $Yb_2Ba_2Sn_6$ sample, and this originates with $Ba_xYb_{3-x}Sn_5$.

Energy-Dispersive X-ray Spectroscopy (EDX) Analyses. EDX measurements were applied to single crystals of the two compounds

(10) Dubois, F.; Schreyer, M.; Fässler, T. F. *Inorg. Chem.* **2005**, *44*, 477.
(11) (a) Bobev, S.; Sevov, S. C. *Inorg. Chem.* **2001**, *40*, 5361. (b) Todorov, I.; Sevov, S. C. *Inorg. Chem.* **2004**, *43*, 6490.
(12) Villars, P.; Calvert, L. D. *Pearson's Handbook of Crystallographic Data for Intermetallic Phases*, 2nd ed.; American Society for Metals International: Metals Park, OH, 1991.
(13) (a) Klem, M. T.; Vaughey, J. T.; Harp, J. G.; Corbett, J. D. *Inorg. Chem.* **2001**, *40*, 7020. (b) Zürcher, F.; Nesper, R.; Hoffmann, S.; Fässler, T. F. *Z. Anorg. Allg. Chem.* **2001**, *627*, 2211.
(14) Leon-Escamilla, E. A.; Corbett, J. D. *Inorg. Chem.* **1999**, *38*, 738.
(15) Fässler, T. F; Hoffmann, S. *Z. Anorg. Allg. Chem.* **2000**, *626*, 106.
(16) Hoffmann, S.; Fässler, T. F. *Inorg. Chem.* **2003**, *42*, 8748.
(17) Eisenmann, B.; Schaefer, H.; Turban, K. *Z. Naturforsch.* **1975,** *30B*, 677.
(18) Echerlin, P.; Leicht, E.; Wölfel, E. *Z. Anorg. Allg. Chem.* **1961**, *307*, 145.
(19) Merlo, F.; Fornasini, M. L. *J. Less-Common Met*, **1967**, *13*, 603.
(20) Miller, G. J. Private communication.
(21) Ganguli, A. K.; Guloy, A. M.; Leon-Escamilla, E. A.; Corbett, J. D. *Inorg. Chem.* **1993**, *32*, 4349.

Table 1. Some Crystal and Refinement Data for $Yb_2Ba_2Sn_6$ and $Ca_2Ba_2Sn_6$

empirical formula	$Yb_2Ba_2Sn_6$	$Ca_2Ba_2Sn_6$
fw	1332.9	1067.0
space group, Z	*Cmca*, 8	*Cmca*, 8
a (Å)	15.871(3)	15.912(3)
b (Å)	9.387(2)	9.497(2)
c (Å)	17.212(3)	17.184(3)
V (Å^3)	2564.3(9)	2597.0(9)
ρ (Mg/m^3)	6.905	5.458
μ (mm^{-1})	31.87	18.03
R1, wR2 [$I > 2\sigma(I)$][a]	0.0307, 0.0770	0.0285, 0.0525
R1, wR2 (all data)	0.0332, 0.0784	0.0384, 0.0549

[a] $R1 = \sum||F_o| - |F_c||/\sum|F_o|$; $wR2 = \{\sum[w(F_o^2 - F_c^2)^2]/\sum[w(F_o^2)^2]\}^{1/2}$, in which $w = 1/[\sigma^2(F_o^2) + (0.0302P)^2 + 5.74P]$, $P = (F_o^2 + F_c^2)/3$.

Table 2. Atomic Coordinates and Equivalent Isotropic Displacement Parameters ($\times 10^3$, Å^2)

atom	site	x	y	z	U(eq)
			$Yb_2Ba_2Sn_6$		
Ba1	8*f*	0	0.1742(1)	0.4141(1)	16(1)
Ba2	8*d*	0.2160(1)	0	0	15(1)
Sn1	8*f*	0	0.2817(1)	0.2197(1)	14(1)
Sn2	8*f*	0	0.0657(1)	0.0854(1)	14(1)
Sn3	16*g*	0.1185(1)	0.3157(1)	0.0927(1)	15(1)
Sn4	16*g*	0.2767(1)	0.2359(1)	0.1633(1)	16(1)
Yb	16*g*	0.1341(1)	0.0114(1)	0.2281(1)	15(1)
			$Ca_2Ba_2Sn_6$		
Ba1	8*f*	0	0.1761(1)	0.4141(1)	16(1)
Ba2	8*d*	0.2170(1)	0	0	15(1)
Sn1	8*f*	0	0.2797(1)	0.2184(1)	13(1)
Sn2	8*f*	0	0.0681(1)	0.0847(1)	14(1)
Sn3	16*g*	0.1184(1)	0.3148(1)	0.0919(1)	14(1)
Sn4	16*g*	0.2765(1)	0.2358(1)	0.1631(1)	15(1)
Ca	16*g*	0.1345(1)	0.0094(2)	0.2287(1)	15(1)

to further confirm their compositions. For $Yb_2Ba_2Sn_6$, the results for three selected single crystals indicate the presence of Yb/Ba/Sn in an average molar ratio of 2.06:2.08:5.86. For $Ca_2Ba_2Sn_6$, the results from three selected single crystals gave an average molar ratio of Ca/Ba/Sn of 1.77:1.99:6.24. According to the EDX results, both compounds are very air sensitive and had some tin on their surfaces because of oxidation, in spite of the use of a vacuum-transfer device.

Single-Crystal Structure Studies. Silver-gray crystals of each compound with dimensions of around 0.09 × 0.15 × 0.15 mm^3 were sealed into thin-walled glass capillaries under a nitrogen atmosphere. Data collections were performed on a Bruker SMART APEX CCD diffractometer (Mo Kα radiation, graphite monochromator) at ~293 K. Initial cell constants and an orientation matrix for data collection were determined from the least-squares refinements of the setting angles of 25 centered reflections. Diffraction data for both phases were collected over the angular range 4.74° < 2θ < 56.52° in four sets of 600, 435, 230, and 50 frames with exposure times of 10 s per frame.

The diffraction data were corrected for Lorentz and polarization effects and for absorption with SADABS.[22] A second crystal of each compound was also picked from a different reaction product and refined to confirm the structure. The space group for these two compounds was determined to be *Cmca* (No. 64) on the basis of systematic absences, *E*-value statistics, and the satisfactory refinements of the structures. These were solved by direct methods (SHELXS), which revealed all Ba, Yb or Ca, and Sn atoms. Ultimately, their atomic coordinates and anisotropic thermal parameters were refined by least-squares methods on F^2 with the aid of the SHELXL package.[23] All atomic sites are fully occupied according to separate site-occupancy refinements. Final difference Fourier maps showed featureless residual peaks of 3.32 and −1.84 e/Å^3 for $Yb_2Ba_2Sn_6$ and 1.17 and −1.33 e/Å^3 for $Ca_2Ba_2Sn_6$. Some data collection and refinement parameters are summarized in Table 1. The atomic coordinates and important distances are listed in Tables 2 and 3, respectively. More details of the crystallographic studies and anisotropic displacement parameters are given in the Supporting Information (CIF).

Table 3. Selected Interatomic Distances (Å) in $Yb_2Ba_2Sn_6$ and $Ca_2Ba_2Sn_6$

atom 1	atom 2	$d(Yb_2Ba_2Sn_6)$	$d(Ca_2Ba_2Sn_6)$
Ba1	Sn1	3.495(1)	3.504(1)
	Sn3 (×2)	3.606(1)	3.5911(8)
	Sn2	3.674(1)	3.723(1)
	Sn2	3.828(1)	3.808(1)
	Sn4 (×2)	3.8296(9)	3.8375(8)
	Sn3 (×2)	3.857(1)	3.916(1)
Ba2	Sn3 (×2)	3.5264(8)	3.5287(7)
	Sn3 (×2)	3.7041(8)	3.7275(8)
	Sn4 (×2)	3.7050(8)	3.7106(7)
	Sn4 (×2)	3.7496(8)	3.7632(7)
	Sn2 (×2)	3.7802(9)	3.8026(8)
M	Sn4	3.1527(8)	3.166(2)
	Sn4	3.1530(7)	3.176(2)
	Sn1	3.1605(8)	3.188(2)
	Sn4	3.2871(8)	3.317(2)
	Sn2	3.2896(8)	3.318(1)
	Sn1	3.3145(8)	3.347(2)
	Sn3	3.5993(9)	3.604(2)
	Sn3	3.6945(8)	3.742(2)
Sn1	Sn3 (×2)	2.9012(9)	2.8949(8)
	Sn2	3.075(1)	3.052(1)
	Yb (×2)	3.1605(8)	3.188(2)
	Yb (×2)	3.3145(8)	3.347(2)
	Ba1	3.495(1)	3.504(1)
Sn2	Sn3 (×2)	3.0106(9)	3.0088(9)
	Sn1	3.075(1)	3.052(2)
	Sn2	3.186(2)	3.186(2)
	Yb (×2)	3.2896(8)	3.318(2)
	Ba1	3.674(1)	3.723(1)
	Ba2 (×2)	3.7802(9)	3.8026(8)
	Ba1	3.828(1)	3.808(1)
Sn3	Sn4	2.8879(9)	2.8965(7)
	Sn1	2.9012(9)	2.8949(8)
	Sn2	3.0106(9)	3.0088(9)
	Ba2	3.5264(8)	3.5287(7)
	Yb	3.5993(9)	3.604(2)
	Ba1	3.606(1)	3.5911(8)
	Yb	3.6945(8)	3.742(2)
	Ba2	3.7041(8)	3.7275(8)
	Ba1	3.857(1)	3.916(1)
Sn4	Sn3	2.8879(9)	2.8965(7)
	Sn4	3.103(1)	3.104(1)
	Yb	3.1527(8)	3.166(2)
	Yb	3.1530(7)	3.176(2)
	Yb	3.2871(8)	3.317(2)
	Ba2	3.7050(8)	3.7106(7)
	Ba2	3.7496(8)	3.7632(7)
	Ba1	3.8296(9)	3.8375(8)

Theoretical Calculations. The band structures for $M_2Ba_2Sn_6$ (M = Yb, Ca) were calculated by extended Hückel and TB-LMTO-ASA methods with the aid of the crystal and electronic structure analyzer (CAESAR) package[24] and the Stuttgart LMTO47[25]

(22) Blessing, R. H. *Acta Crystallogr.* **1995**, *A51*, 33.

(23) *SHELXTL*; Bruker AXS, Inc.; Madison, WI, 2000.

(24) Ren, J.; Liang, W.; Whangbo, M.-H. *CAESAR for Windows*; Prime-Color Software, Inc.: North Carolina State University: Raleigh, NC, 1998.

(25) van Schilfgarde, M.; Paxton, T. A.; Jepsen, O.; Andersen, O. K.; Krier, G. *Program TB-LMTO*; Max-Plank-Institut fur Festkorperforschung; Stuttgart, Germany, 1994.

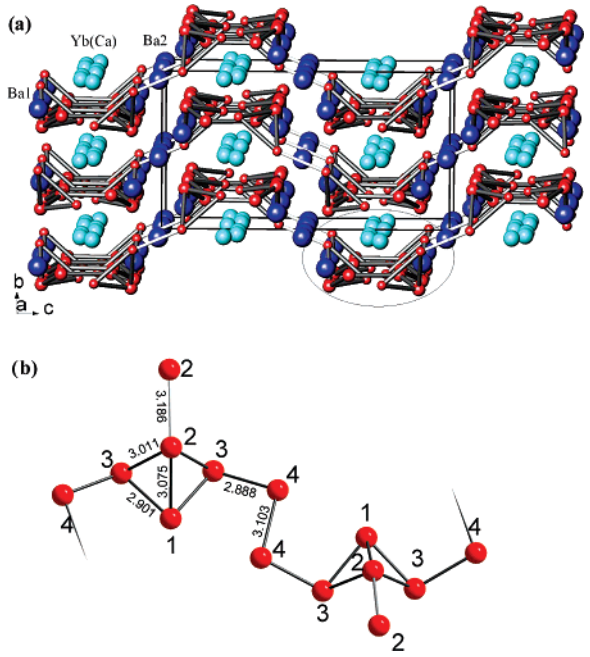

Figure 1. Crystal structure of $M_2Ba_2Sn_6$ (M = Yb, Ca). (a) Three-dimensional view of [−100]. (b) The repeat unit for the tin chain with bond distances (Å) marked for$Yb_2Ba_2Sn_6$.

Figure 2. Polyanions containing butterfly shapes. (a) Isolated butterfly in Ba_3Si_4.[26] (b) Polymeric chains of butterfly anions in α-Ba_3Ge_4.[27]

program, respectively. Yb 4f orbitals were treated as core in the latter calculations. The atomic parameters used in the former calculations are presented in the Supporting Information.

Results and Discussion

Structure Description. The isostructural title compounds $Yb_2Ba_2Sn_6$ (**1**) and $Ca_2Ba_2Sn_6$ (**2**) crystallize in space group *Cmca* (No. 64), Pearson symbol oC80. Both contain Sn polyanions composed of infinite zigzag chains along $\vec{a}$ that are stacked in parallel along $\vec{b}$, Figure 1a. These chains are further connected, principally along $\vec{c}$, through an additional contact between Sn2 atoms in adjoining chains to form corrugated layers of chains. The repeat unit in the tin chain shown in Figure 1b consists of a tetrameric butterfly unit of 3b (3-bonded) Sn^- interconnected by pairs of bridging 2b-$Sn4^{2-}$. Thus, each infinite tin chain can be described in terms of the repeat units {−Sn4−[Sn3−Sn1−Sn2−Sn3]−Sn4−}$_n$, which would have a closed shell charge of −8 according to classical octet binding concepts. Butterfly arrangements alone can be found as isolated anions Si_4^{6-} in Ba_3Si_4[27] and in chainlike cross-linked polymers of butterfly anions of Ge_4^{6-} in α-Ba_3Ge_4,[28] Figure 2. The configurations of adjacent pairs of tin chains along the *b* axis in Figure 1a alternate according to screw axes along *x*, 0, 1/4, etc. This

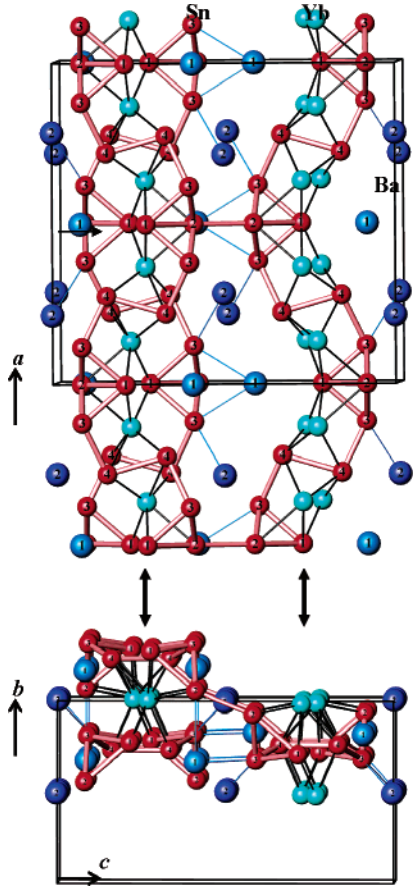

Figure 3. [100] views of three tin chains at the bottom (compare Figure 1a) aligned with the corresponding [010] elevations of the same units at the top. The Yb atoms (lighter blue) interbridge adjacent pairs of chains as shown on the left for two chains about a single string of Yb and on the right for two strings of Yb about a single tin chain. The serpentine natures of displaced tin chains that follow screw axes along *x*, 0, 1/4, etc., are evident in the top left view, as well as the interchain bridges between butterfly units that are centered at 1/2, 0, 1/2, etc. Each Yb is 6-bonded to Sn in two chains at 3.15−3.31 Å, as marked.

important feature is clarified in Figure 3 in terms of the [100] view along three tin chains at the bottom aligned with the corresponding [010] elevation of the same units at the top. The lighter blue Yb atoms can be seen to intimately interbridge adjacent pairs of chains, which are shown on the left as two chains about a single string of Yb and on the right as two arrays of Yb about a single tin chain. The serpentine nature of adjacent tin chains displaced by *a*/2 can be readily perceived in the top left view, as well as the alternating interchain bridges between butterfly units that are centered at 1/2, 0, 1/2, etc. Each Yb is 6-bonded to Sn in two chains at 3.15−3.31 Å, as marked. These Sn−Yb functions are significant in the bonding considerations, as will be noted later. (The shortest Ba−Sn interactions are also marked. More detail is given in Supporting Information, Figures S1 and S2.)

The surroundings about one tin layer viewed along [010] are marked in Figure 4, which is more helpful for the locations of Ba. The large spaces opposite the Sn2−Sn2 bonds contain the Ba1 atoms, whereas the Ba2 atoms locate at (*x*, 0, 0) between pairs of chains. The somewhat longer Sn2−Sn2 bonds that interconnect separate chains obliquely

(26) Eisenmann, B.; Janzon, K.H.; Schaefer, H.; Weiss, A. *Z. Naturforsch.* **1969**, *24*, 457.
(27) Zürcher, F.; Nesper, R. *Angew. Chem., Int. Ed.* **1998**, *37* (23), 3314.
(28) Shannon, R. D. *Acta. Crystallogr.* **1976**, *A32*, 751.

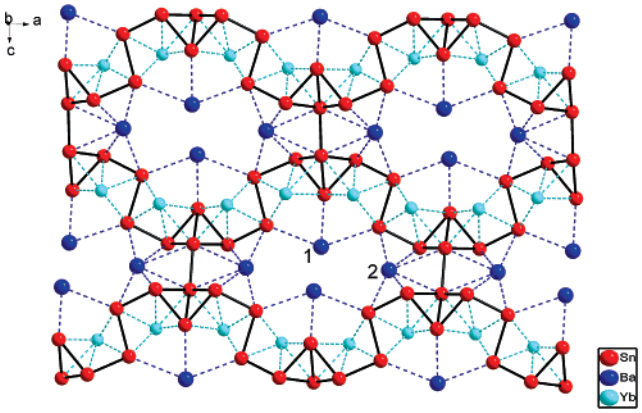

Figure 4. [010] projection of one puckered tin layer with Yb (Ca) and Ba surroundings. The coordination of Yb and Ba about Sn (for distances below 4.0 Å) are marked by dotted lines (Ba1−Sn2 lies in another layer).

along the $\vec{c}$ direction are doubtlessly caused in part by the size of Ba2. The structure can also be viewed from another perspective: smaller Yb (Ca) atoms stuffed between pairs of tin chains to form [M2Sn6] layers, which stack along *b* into a pseudo-2D close-packed array, Figure 1a. The bonding Sn−Sn distances in and between the tin chains vary between 2.89 and 3.18 Å in both phases; the Sn−Sn distances in $Yb_2Ba_2Sn_6$ are marked in Figure 1b. The distances within the tin chains are consistent with those in other tin compounds.

The details of the distance aspects in the compounds are relatively complex, reflecting packing and interactions between the tin chains and two differently sized cations and, less clearly, the disparate formal charges of the tin atoms in the chain. Both the crystal radii[28] of Ca^{2+} or Yb^{2+} and the comparative distances in the two products are very close. The fact that d_{Sn-Sn} is ∼0.02 Å smaller with Ca but d_{M-Sn} is larger with Ca and so is the unit cell volume of the Ca phase suggests that the Ca−Sn interactions may be slightly weaker, although this is not particularly evident from the calculations. On the other hand, standard radii for M^{2+} and Ba^{2+} differ by ∼0.28 Å, and this is clearly seen in their relative segregation in the structures, Figures 1a and 4, as well as in the stability of the phase. Formal charges on different Sn atoms in the chain become more negative with increased numbers of formal electron pairs thereon. Thus, the more polar Yb(Ca)−Sn interactions might also be manifest in the structures. But the numbers of Yb (Ca) neighbors about each Sn do not always so vary, that is, for Sn1(−1), 4Yb; Sn4(−2), 4Yb; Sn2(0), 2Yb; and Sn3(−1), 0Yb. This basically electrostatic interpretation neglects both the complex packing and the parallel and clearly important covalent contributions revealed by theory (below).

Interactions of lone pairs of electrons across bonds are thought to be important as well, and in fact, the three longest distances within the chains are indeed associated with the larger numbers of Yb neighbors about those tin pairs, there being six Yb about both Sn4−Sn4 (3.1 Å) and Sn1−Sn2 (3.08 Å) separations, whereas the long Sn2−Sn2 interchain bond is surrounded by four Yb neighbors, as well as by Ba. However, substantial covalency effects appear dominant, as considered in the next section. Overall, Ba1 and Ba2 are

Table 4. −ICOHP Values (eV/bond) for Sn−Sn Interactions in $M_2Ba_2Sn_6$ (M = Yb, Ca)

	$Yb_2Ba_2Sn_6$		$Ca_2Ba_2Sn_6$	
bond	distance (Å)	−ICOHP	distance (Å)	−ICOHP
Sn3−Sn4	2.888	2.18	2.897	2.17
Sn3−Sn1	2.901	1.97	2.895	2.00
Sn2−Sn3	3.011	1.56	3.009	1.58
Sn1−Sn2	3.075	1.09	3.052	1.17
Sn4−Sn4	3.103	1.52	3.104	1.54
Sn2−Sn2[a]	3.186	0.89	3.186	0.89

[a] Interchain bond.

nine- and ten-coordinate over a range of 3.5−3.9 Å (Figure S1, Supporting Information), and their covalency with Sn appears to be relatively small.

Bonding Analysis. The two title compounds can be easily rationalized by the assignments $2Ba^{2+}$, $2Yb^{2+}$ (Ca^{2+}), and $[Sn_6]^{8-}$ for the isolated chain according to the Zintl−Klemm concept.[1] However, the interlayer Sn2−Sn2 distance of 3.19 Å is only 0.08 Å greater than the longest within the chain, and comparable Sn−Sn bond distances have been reported in some other compounds, for example, 3.16 Å in Sn−Sn dimers in $Yb_{36}Sn_{23}$,[14] in which there are packing problems as well. To clarify this problem, Mulliken overlap populations (Supporting Information) and ICOHP values (Table 4) for all Sn−Sn bonds were calculated by the respective extended Hückel and LMTO methods. Both assessments reveal that Sn2−Sn2 contacts are comparable to those within the tin chains, which classically then means the products are metallic Zintl phases.[1b,29−34] Figure 1b shows that the tin chain has one 4b-Sn2(0), two 3b-Sn3(−1), one 3b-Sn1(−1), and two 2b-Sn4(−2). If the oxidation states of Yb, Ca, and Ba are considered to be +2, $(Yb, Ca)_2Ba_2Sn_6$ is one electron rich per formula unit [8−0−2(1)−1−2(2) = 1], in agreement with the metallic property reflected by the following calculations.

LMTO calculations were performed on both compounds to examine the band structure of the tin chain and the participation of cations in the overall bonding. Results for both are very similar in terms of both projected DOS for the whole structure and the separate contributions from the constituent elements, and so only data for $Yb_2Ba_2Sn_6$ are shown in Figure 5. E_F cuts the DOS at a low but nonzero trough, which indicates both phases are metallic, although the pseudogaps indicate the phase is nearly closed shell here rather than at the Zintl limit. Yb 5d, Ba 5d, and Sn 4p all show considerable contributions to the bands around the Fermi level, whereas Ba and Sn s states are important only below ∼ −4 eV (compare Figure 6). The lower dotted line marks E_F for one fewer electron per formula unit (8e/cell), presumably at the top of the ideal valence band. The extra metallic electron is presumably accommodated principally

(29) Lam, R.; Mar, A. *Solid State Sci.* **2001**, *3*, 503.
(30) Bobev, S.; Bauer, E. D.; Thompson, J. D.; Sarrao, J. L.; Miller, G. J.; Eck, B.; Dronskowski, R. *J. Solid State Chem.* **2004**, *177*, 3545.
(31) Dong, Z.-C.; Corbett, J. D. *J. Am. Chem. Soc.* **1995**, *117*, 6447.
(32) Rodriguez-Fortea, A.; Canadell, E. *Inorg. Chem.* **2003**, *42*, 2759.
(33) Mudring, A.-V.; Corbett, J. D. *Inorg. Chem.* **2005**, *44*, 5636.
(34) Alemany. P.; Llunell, M.; Canadell, E. *Inorg. Chem.* **2006**, *45*, 7235.

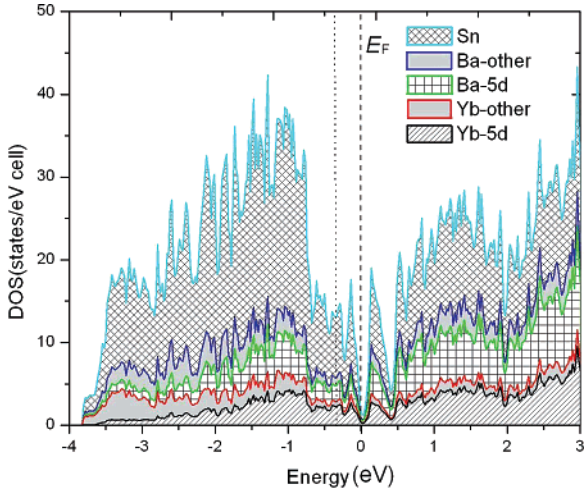

Figure 5. Graphical representation of the results of the TB-LMTO-ASA studies for $Yb_2Ba_2Sn_6$ with the projected densities of states (PDOS) for Yb-d and Ba-d and other contributions as in the legend. Total density of states is the sum of these PDOSs; in other words, the individual contributions are stacked so the areas correctly reflect the proportions. E_F corresponds to the experimental 32 valence electrons/formula unit, and the dotted line marks the position of the Zintl phase limit of 31 electrons/formula unit ($Z = 4$).

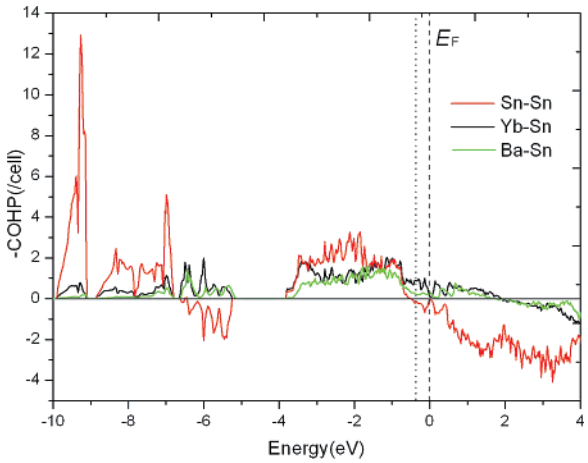

Figure 6. Crystal orbital Hamiltonian population (−COHP) plot for the sum of all Sn−Sn (red), Yb−Sn (black), and Ba−Sn (green) interactions as a function of energy in $Yb_2Ba_2Sn_6$. (The relative numbers are 10:8:6.) The data below −5 eV originate largely with s orbitals.

in the intervening bands which involve mainly Sn 4p, Yb 5d, and Ba 5d orbitals (below).

It is striking that this metallic Zintl phase has such a marked pseudogap and is so close to being closed shell. The octet rule is clearly too crude a starting place. An earlier inquiry into the presence of two extra electrons (and two excess Na^+) per formula unit in the unusual Na_6TlSb_4[31] with an extended ring system by ab initio means revealed that a relatively distinct group of π^* states on Sb plus Na s accommodated the two extra electrons at the top of the σ and π bands for the Tl−Sb rings. The present system shows no clear demarcation in DOS between the supposed tin p and the conduction band holding the extra electrons, an effect that is reflected in the dispersion of the energy bands. Fat band plots (Supporting Information) show similar situations at E_F for both phases, a band of largely Yb (Ca) d and Sn p that pushes above E_F near Γ in the direction of Y, and a second band with these contributions plus Ba d that pushes down at Y, a classical semimetal signature. It is a little surprising that there is no more differentiation between Ca 3d and Yb 5d in their bonding capabilities here, as was so obvious in the more reduced Sc_2Te versus Dy_2Te.[34]

To check the interactions between atoms, a variety of crystal orbital Hamilton population functions (−COHP) were evaluated. To quantify the interactions between atoms, the integrated crystal overlap Hamiltonian populations (−ICOHP) were also determined (Table 4). The ICOHPs obtained from the first principle LMTO methods are better measures of relative bond strengths than the Mulliken overlap populations (MOPs) from extended Hückel calculations. The −ICOHP values are about 0.8 eV/bond over all Yb−Sn or Ca−Sn contacts, which are of the same magnitude as for the respective Sn2−Sn2 bonds (0.89 eV/bond). An especially strong interaction is found for Yb(Ca)−Sn2, 1.1 eV/bond, which likewise suggests a considerable cation involvement in the interchain bonding. The respective −ICOHP values for the internal Sn1−Sn2 bonds in the butterfly are 0.91 (Yb) and 1.17 (Ca) eV/bond. Furthermore, according to the band structures, Yb(Ca) d orbitals show substantial contributions to the states around the Fermi level (Figure 5) and to Yb(Ca)−Sn bonding in these compounds. Fat band representations for Yb (Ca) contributions to the bands (Supporting Information) illustrate a general and significant involvement of the cations in most of the valence bands (and above).

Total Sn−Sn, Yb−Sn, and Ba−Sn COHP curves for $Yb_2Ba_2Sn_6$, Figure 6, give more insight and details regarding the bonding in the whole structure. All are roughly optimized at E_F, Yb−Sn being the greatest, but there are still some empty cation−tin bonding states above Fermi. Interestingly, the crucial Sn−Sn bonding is optimized even somewhat below the p-band limit (31e/formula unit, dotted) and is mainly antibonding above there. COHP curves were also calculated for each separate Sn−Sn and Yb(Ca)−Sn interaction. Figure 7a shows that the antibonding effects below Fermi are associated mostly with the somewhat longer Sn4−Sn4 and Sn2−Sn2 bonds, whereas bonding in short Sn1−Sn2 and Sn2−Sn3 (not shown) separations are (naturally) almost fully optimized. The Yb−Sn results for the five shortest bonds, Figure 7b, and the smaller Ba−Sn increments (SI) show that all are bonding at and below E_F.

The results also give us some interesting insights regarding the sort of states occupied by the one extra electron per $Ba_2M_2Sn_6$. These are presumably situated more or less at the top of the Sn valence p band and just below E_F. (Certainly not simply on the cations, which would put them at much higher energies.) COHP curves for selected Sn−Sn and Yb−Sn bonds in Figure 7 combined with DOS data in this region gave us this information. The largest increments in the DOS (Figure 5) are for total Sn (blue) which may be bonding or antibonding, followed by Ba 5d (green) and Yb 5d (black), particularly around 0.15 eV. Figure 7a shows that these particularly involve antibonding Sn2−Sn2 and Sn4−Sn4 states for the two longest bonds, the latter also having the largest number of formal lone pairs. On the other hand, Sn1−Sn2 (the "body" of the butterfly, one nominal lone pair) is

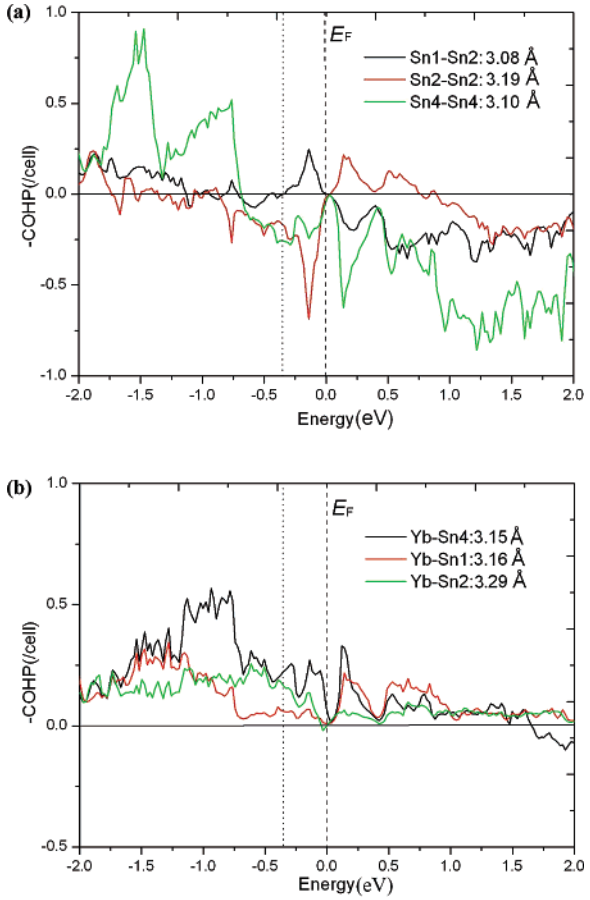

Figure 7. Crystal orbital Hamiltonian population (−COHP) plot for separate Sn−Sn (a) and Yb−Sn (b) pairs in$Yb_2Ba_2Sn_6$. Note: The scale expansions relative to Figure 6.

appreciably bonding in this region. The loss of bonding in the first two contributions above will be compensated by bonding interactions of the electrons with cations, Figure 7b, which involve, mainly, Yb−Sn4 (three cations and two lone pairs per Sn), followed by lesser Yb−Sn1 for tin atoms that project outward from the chain and have two pair of Yb neighbors. The Ba−Sn −COHP values (Supporting Information) are a good deal smaller, but still bonding, particularly with Sn2 and Sn3. Certainly these particular metallic Zintl compounds are dramatically affected by cation involvement in the bonding of the highest-lying electrons. This may in fact be general for the higher-charged cations that have d-bonding orbitals.

Bonding analyses of this latest type of metallic Zintl phase, that is, compounds with extra bound cations and electrons, give further emphasis to the trade-offs that occur in the dense solid state between optimization of covalent bond energies within the so-called Zintl anions and the total energies that include not only Coulombic terms from their polar constitution but more particular (and less obvious) cation−anion covalent bonding effects. All of these end up in some compromise in the only observable, the most stable phase. It seems fairly logical that the more obscure interion covalent bonding would fall just below E_F or, perhaps, in the upper regions of the p-element valence band, but these aspects have seldom been investigated or established. In the present examples, the binding of the extra and more delocalized electrons originates from combinations of cation valence orbitals, d particularly, with basically what otherwise would be LUMO states from p-element bonding in the Zintl anion or network.[32,33] And the net result is found not in a separable unit or complex but rather in the dense and tightly packed solid-state common for such "polar intermetallic" phases in which high coordination numbers for, rather than directed bonds to, the cations are strongly favored. It is this characteristic that sometimes gives advantage to the used of mixed cation sizes or charges[2] to secure both the "best fit" and a suitably close approximation to the stability limit of the Zintl anion. Mixed anions in the latter can also help realize such favorable situations.[36]

Conclusions

Two new stannides $M_2Ba_2Sn_6$ (M = Yb and Ca) represent new examples of ternary alkaline-earth (rare-earth) metal−tin systems and have novel tin chain substructures. Theoretical calculations indicate these two compounds are metallic but with only a deep pseudogap at the Fermi level. Yb and Ca cations play an important role both in the formation of such metallic Zintl phases according to TB-LMTO-ASA results and in supporting the binding of the excess metallic electrons.

Acknowledgment. The authors thank Gordon J. Miller, Bin Li, and Qisheng Lin for advice on the theoretical calculations. This research was supported by the office of the Basic Energy Sciences, Materials Sciences Division, U.S. Department of Energy. The Ames Laboratory is operated by DOE by Iowa State University under Contract No. DE-AC02-07CH11358.

Supporting Information Available: Refinement parameters for $M_2Ba_2Sn_6$ in CIF format, the atomic parameters used in Extended Hückel calculations, Mulliken overlap populations for Sn−Sn in $M_2Ba_2Sn_6$, the cation coordination environments for Yb−Sn and Ba−Sn, the DOS and COOP results calculated from extended Hückel method, fatbands for Sn-5p, Yb-5d, Ca-5d, and Ba-5d states in both $M_2Ba_2Sn_6$, and COHP data for separate Ba−Sn interactions. This material is available free of charge via the Internet at http://pubs.acs.org.

IC070042P

(35) Herle, P. S.; Corbett, J. D. *Inorg. Chem.* **2001**, *40*, 1858.
(36) Ge, M.-H.; Corbett, J. D. *Inorg. Chem.* **2007**, submitted for publication.